Imaging in the ocean with ambient noise: the ORB experiments

Chad L. Epifanio,[a)] John R. Potter,[b)] Grant B. Deane, Mark L. Readhead,[c)] and Michael J. Buckingham[d)]
Marine Physical Laboratory, Scripps Institution of Oceanography, University of California, San Diego, 9500 Gilman Drive, La Jolla, California 92093-0213

Acoustic daylight imaging is a new technique that has been proposed for creating pictorial images of objects in the ocean from the ensonification provided by the incident ambient noise field. To investigate the feasibility of the technique, a series of experiments was performed from the research platform ORB, moored in San Diego Bay, Southern California. Central to these experiments was an acoustic receiver known as ADONIS (acoustic daylight ocean noise imaging system), which consists of a spherical reflector, 3 m in diameter, with an elliptical array of 130 hydrophones at the focal surface. This system, which is broadband, operating between 8 and 80 kHz, forms a total of 126 receive-only beams spanning the vertical and horizontal. The ambient noise power in each beam is mapped into a pixel on a VDU. Various types of targets were used in the experiments, including planar panels and cylindrical, polyethylene drums containing wet sand, seawater or syntactic foam (essentially air), and most of the experiments were conducted with the targets at ranges between 20 and 40 m. At the time of the experiments the noise field in the area was created primarily by snapping shrimp. Moving, color images of the object space were successfully created with ADONIS. Some representative static images from the moving sequences are presented and discussed in the paper. © *1999 Acoustical Society of America.* [S0001-4966(99)04611-1]

PACS numbers: 43.30.Nb, 43.35.Sx, 43.60.Gk [DLB]

INTRODUCTION

Over recent years, anecdotal evidence has indicated that a submarine can be detected by the acoustic shadow it casts in the ambient noise field. In the mid-eighties, at the suggestion of Allen Ellinthorpe, Flatté and Munk[1] investigated the shadowing phenomenon theoretically and, at around the same time, Buckingham[2] independently introduced the idea that, as the ambient noise field is in many respects analogous to daylight in the atmosphere, it should be possible to create recognizable, pictorial images of objects in the ocean solely through the acoustic illumination provided by the ambient noise. Such ''Acoustic Daylight'' imaging, as Buckingham[2] designated the technique, would be similar to conventional photography, whereby an image of an object is created even though the object itself may not be luminous and no dedicated light source (e.g., a flashgun) is used for illumination. Ambient light (daylight) scattered from the object gives rise to the photographic image, whereas ambient sound would fulfill the same role in the ocean.

To test this idea, Buckingham *et al.*[3] conducted a pilot experiment off Scripps Pier in 1991, the results of which indicated that, at ranges up to 12 m, a rectangular target can be detected solely from the modifications its presence intro-

duces into the ambient noise field. In effect, the targets created an acoustic contrast, that is, a difference in the noise level between the situations where the targets were present and absent. The acoustic detector used for focusing in this experiment was a parabolic dish of diameter 1.2 m, with a piezoelectric hydrophone located at the focal point. The surface of the dish was faced with closed-cell neoprene foam, which is an efficient acoustic reflector (essentially pressure-release) over the operating frequency band from 5 to 50 kHz. When the output of this receive-only, single-beam system is displayed as an intensity map, it forms what is in effect a single-pixel image of the object space. Since they are linked by a one-to-one correspondence, more pixels would require more beams.

The targets in the pilot experiment fully occupied the beam throughout most of the operating frequency range. Much of the ensonification was generated by snapping shrimp located on the pier pilings behind the parabolic dish, a situation analogous to front lighting produced when the sun is behind a (photographic) camera. The acoustic contrast observed in the experiment was around 3 dB, which is comparable with theoretical estimates by Buckingham[4] of the contrast created by a spherical target embedded in plane-wave noise fields showing various degrees of anisotropy. Similar levels of contrast were also obtained by Potter[5] from a numerical simulation of acoustic daylight imaging of volumetric targets in a shallow water channel.

In his wave-theoretic analysis of ambient noise imaging, Buckingham[4] considered a linear array of hydrophones steered to endfire as the acoustic receiver. He found that the maximum contrast occurs when the angle subtended by the spherical target at the receiver matches the angular beam-

width (as measured between the -3 dB points) of the detection system. In this case, if the beamwidth is greater than the angle subtended by the target, background noise enters the beam, which reduces the contrast, while a beamwidth that is smaller than the subtended angle leads to rejection of scattered energy, again reducing the contrast. This observation provides a guide to imaging system requirements but should not be interpreted as a universally valid criterion of image quality: no such metric is known that is independent of the source distribution.[6]

Makris et al.[7] have developed a theoretical model of ambient noise imaging in a shallow water waveguide. They considered a spherical target at mid-depth in the water column, with the focusing performed by a planar, billboard array. When the beamwidth (approximately) matched the angular width of the target, they found that the contrast in the resultant image was 3.6 dB (bottom left panel of their Fig. 12), which is comparable with the results of Buckingham[4] and Potter.[5] With a significantly broader beam, however, the contrast fell to 0.35 dB (bottom right panel of their Fig. 12), which is also consistent with the previous theoretical investigations.[4,5]

The spatial scale that is resolved in an acoustic daylight image will, of course, be determined by the beamwidth of the acoustic detection system, in accord with the Rayleigh resolution criterion. To create a multiple-pixel image, some form of multi-beam or beam-scanning receiver system is required: the scattered acoustic energy from the object space must be sampled over a range of arrival angles. Clearly, the single-beam system used in the pilot experiment at Scripps Pier is not satisfactory for such an application.

To fulfill the imaging requirement, a performance specification for a prototype multi-beam receiver was drawn up. It was decided that the system should have 100 or more beams, a decade of bandwidth, a beamwidth at the highest operating frequency of less than 1 degree, corresponding to a spatial resolution of better than 1.75 m at a range of 100 m, and rear baffling to prevent unwanted noise from behind the receiver corrupting the response. All these requirements were incorporated into the acoustic daylight ocean noise imaging system (ADONIS), which was designed and built at Scripps over a period of about 2 years between 1992 and 1994.[8,9] In this article, ADONIS is described briefly and a selection of ambient-noise images of planar and volumetric targets, obtained during two deployments in San Diego Bay, southern California, in August 1994 and October 1995, are discussed. These deployments have come to be known as the ORB experiments.[10]

I. ADONIS

Figure 1 shows a schematic of the ADONIS multi-beam receiver. Mechanically, the system consists of a spherical acoustic reflector with both a radius of curvature and a diameter of 3 m. The dish itself is a spherical fibreglass shell, the concave side of which is faced with closed-cell neoprene foam, selected because it is an almost perfect (pressure-release) acoustically reflecting material. A steel framework provides the dish with structural rigidity. The dish assembly is mounted on a vertical mast, which stands on a horizontal,
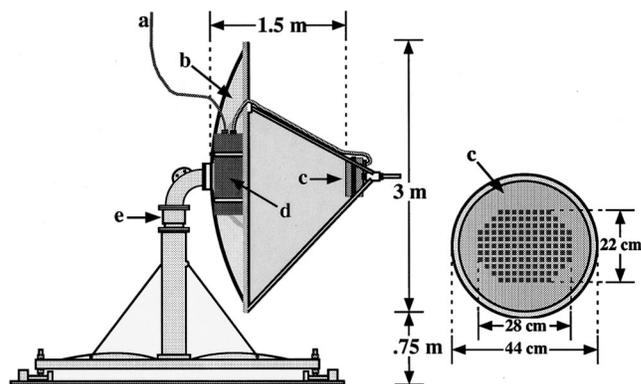

FIG. 1. Schematic of ADONIS. (a) Umbilical cable which provides power to the system and transmits data to a desk-top computer at the surface. (b) Spherical reflector faced with low density, closed cell neoprene foam. (c) 130-element hydrophone array, showing the elliptical configuration of the sensors, which have a center to center spacing of 2 cm. (d) Electronics canister where filtering is performed and frames are constructed. (e) Supporting mast containing a coaxial hydraulic motor for rotating the dish in azimuth.

triangular base frame. At the corners of the base frame are height-adjustable legs, which divers use for leveling the system after it has been deployed on the seabed. Inside the mast is a remotely controlled, coaxial hydraulic motor, which is capable of rotating the dish around a full 360 degrees in the horizontal. This facility is useful for panning the dish across the object space, and for monitoring the horizontal directionality of the ambient noise field.

The acoustic sensing is performed by an array of 130 piezoelectric hydrophones arranged in an approximately elliptical configuration, with the major (horizontal) and minor (vertical) axes containing 14 and 11 sensors, respectively. Each of the sensing elements has a square cross section with center-to-center spacing of 2 cm. The face of the array of sensors is slightly convex to match the curvature of the focal region of the spherical reflector. This and many other design details of the dish and the sensor array were established with the aid of a suite of simulation software packages that were developed at the outset of the project.

A multi-element reflector is an unusual design for an acoustic receiver. From the point of view of ambient noise imaging, it has the advantage that the beam forming is performed as a natural consequence of the geometry of the system: no phase or time delays are necessary. Sound incident on the dish from a given direction is focused onto a particular hydrophone, or, conversely, a given sensor has a unique ''look'' direction, which is governed by its position in the array head. Thus, the 130 hydrophones in the array provide a total of 130 receive-only beams, which are distributed in the vertical and horizontal (although only 126 beams are used for forming images). From the symmetry of the system, the beam widths in the vertical and horizontal are essentially the same. Incidentally, all the hydrophones in the array are off-axis, and the system suffers some degree of aberration arising from scattering by the rim of the dish. A spherical reflector was selected because the aberrations associated with the off-axis sensors are rather less pronounced than those encountered with a parabolic dish. (Of course, with an on-axis

sensor a parabolic dish provides ideal focusing and is thus the preferred choice. Such a system was used in the pilot experiment off Scripps Pier.[3])

ADONIS operates over one decade of bandwidth (cf. one octave for the human eye), extending from 8 to 80 kHz. At the highest frequency the beamwidth between the -3 dB points is 0.75 degrees, which increases to 3.5 degrees at the lowest frequency. The beam centers are independent of frequency, providing an overall angle of view of approximately 10 degrees in the horizontal and 8 degrees in the vertical. In the lower frequency ranges the beams overlap, as a result of which the information they contain is no longer independent. The top frequency of 80 kHz was selected on the grounds that, beyond 80 kHz, the dominant noise component in the ocean was expected to be thermal noise,[11] which contains no imaging information. It is interesting to note, however, that the theoretical limit of around 80 kHz for the onset of thermal noise applies only on the assumption of a true point receiver. In reality, a receiver of finite size will have the effect of reducing the thermal noise fluctuations through surface averaging,[12] thereby increasing the frequency at which thermal noise becomes dominant. This offers the prospect of increasing the upper frequency limit to around 150 kHz in future ambient noise imaging systems.

The geometrical focusing performed by the dish provides a gain of approximately 22 dB at the highest frequency of 80 kHz, which is important in amplifying the very low-level signals scattered from the target. The gain of the dish is defined as the intensity of the acoustic field in the focal region divided by the intensity of the direct-path arrival at the same position. As with any lens system, the position of the focal point relative to the dish varies with the range to the target. Focusing is achieved by racking the hydrophone array in and out relative to the center of the dish in much the same way as the focusing on an optical camera is performed by moving the lens back and forth relative to the film plane.

The broad bandwidth of ADONIS offers the prospect of exploiting ''acoustic color'' for the classification of targets. For example, an object that scatters low frequencies better than high could appear as red in the final image, whereas a good high-frequency scatterer could appear as blue. Thus, it may be possible to distinguish, say, a hollow shell from a solid object of similar shape simply from the different colors of their images.

To show acoustic color in the images, a spectral analysis of the signal in each channel must be performed. Rather than applying a computationally demanding digital fast Fourier transform (FFT) to each channel, an analog technique is used in ADONIS in which a bandpass filter with a constant Q of 4 is swept over the full bandwidth 25 times per second (the frame rate). This task is performed by a bank of 130 switched-capacitor analog filters (one for each sensor channel), which sample the level of the signal at 16 frequency points, or bins, uniformly spaced logarithmically across the frequency band. Figure 2 shows the filter frequency responses; the center frequencies are listed in Table I.

A given frequency bin is sampled simultaneously in all channels. The sampling across the frequency bins is performed sequentially in time, and at each frequency the signal
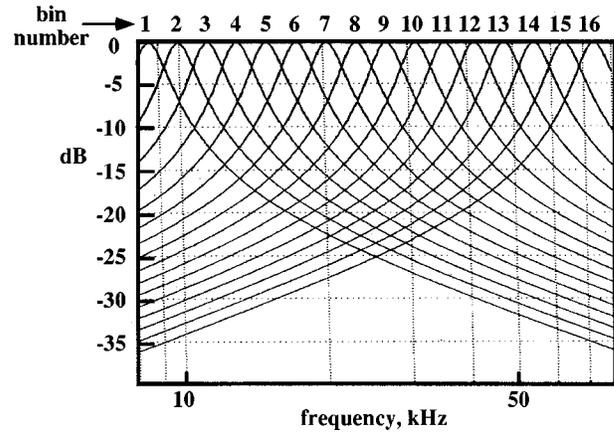

FIG. 2. Frequency responses of the sixteen switched capacitor filters, each normalized to the maximum response.

is allowed to settle before its average is taken over an interval of approximately 1 ms. The time for the complete 16-bin sweep is 40 ms, which sets the 25-Hz frame rate. Thus, each spectral estimate is obtained over an interval that is $\frac{1}{40}$ of the frame acquisition time. From a weighted sum of the resultant 16 intensities, a color is selected from a color palette and applied to the appropriate pixel on a monitor screen. At any instant, the 126 pixels on the screen constitute one image, or frame, in a sequence of continually refreshed static images. The frame rate of 25 Hz is sufficiently rapid to provide smoothly flowing movement in the final videolike output.

It became apparent during the initial ORB deployments that, because of an impedance mismatch, the switched capacitor filters had trouble driving the following stage when operating in the upper 60% of their dynamic range. As a result, the system shows a nonlinear response, which manifests itself as a reduction in contrast between pixels. However, only 25% of the data lie in the upper 60% of the dynamic range, where the effect is most severe. In most of the examples presented below, the nonlinear data were removed prior to creating the images.

The raw (uninterpolated) images are produced in real time on a desktop computer, which also handles data acqui-

TABLE I. Center frequencies at which the intensity of the noise is sampled in each channel, 25 times per second.

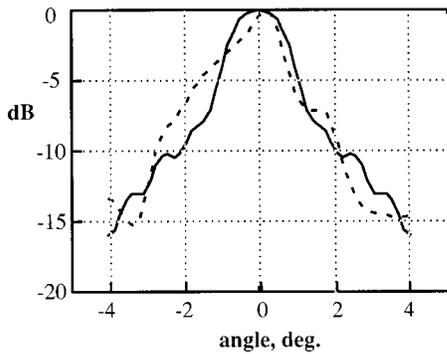| Bin	Frequency (kHz)
1	8.5
2	10.0
3	11.7
4	13.8
5	16.0
6	18.6
7	21.3
8	24.6
9	28.3
10	32.6
11	37.5
12	43.1
13	49.5
14	57
15	64.4
16	75.0

FIG. 3. Example of the measured (dashed) and theoretical (solid) in-air beam pattern taken at a frequency of 8.5 kHz (corresponding to 37.5 kHz in water).
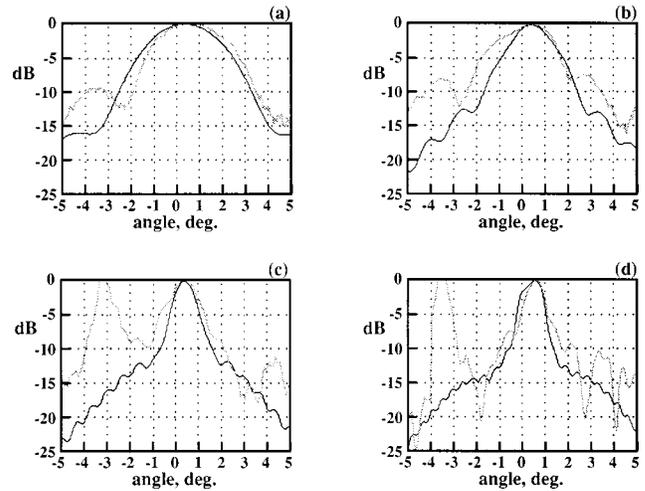

FIG. 4. Measured (gray) and theoretical (black) beam patterns of an array element close to the axis of the dish. (a) 10 kHz; (b) 25 kHz; (c) 50 kHz; and (d) 75 kHz. The array was focused at 25 m, as in the imaging experiments, and the source was at 40 m. The peak to the left of the main lobe in experimental traces (c) and (d) is due to boat noise.

sition and storage. As part of the image processing, a number of refinements are available, including various averaging and normalizing schemes for enhancing image stability. In post-processing, the raw data are interpolated by a factor of 5, that is, five additional points are included between data points, which leads to a significant improvement in the visual quality of the images.

II. BEAM PATTERNS OF ADONIS IN AIR

Before deploying ADONIS in the ocean, the beam patterns of the dish were measured at several frequencies in air on Scripps Pier. The frequency was scaled down appropriately to compensate for the difference between the speed of sound in water ($\approx$1500 m/s) and in air ($\approx$340 m/s). A microphone was mounted in the focal region on the axis of the dish, and the system was panned past a harmonic acoustic source at a range of approximately 30 m. The closed-cell neoprene foam facing the dish was absent during these in-air tests, thus exposing the underlying spherical fiberglass shell, which is essentially rigid.

Figure 3 shows an example of the measured in-air beam pattern at a frequency of 8.5 kHz, corresponding to a wavelength of 4 cm and an equivalent in-water frequency of 37 kHz. The slight asymmetry about the beam center in the measured curve is due largely to a breeze that was blowing across the axis of the dish. For comparison with the measurement, a theoretical beam pattern, derived from an analytical model developed by Deane[13] specifically for this purpose, is also shown in Fig. 3. It can be seen that the theory and measurement show reasonably good agreement. Notice that at this frequency the beam width at the -3 dB points is only 2 degrees. A similar level of agreement was observed at the remaining frequencies for which measurements were performed.

III. BEAM PATTERNS OF ADONIS IN WATER

The beam patterns of ADONIS were measured in water by placing a spherical acoustic source at a range of 40 m and panning the dish across it in both directions, from left to right and right to left. For these tests the pressure-release, closed-cell, neoprene foam facing was present on the dish, as was the case for all the underwater imaging experiments. The

dish was focused to 25 m, with a depth of field extending from 15 to 40 m, which was also the setup used for imaging with ADONIS.

Figure 4 shows examples of the measured beam patterns, at frequencies of 10, 25, 50, and 75 kHz, of a single element located near the geometrical center of the array. For comparison, the theoretically predicted beam patterns[12] are included in the figure. It is evident that the agreement between the theoretical and measured main lobes is reasonable at all four frequencies. Notice that the observed beamwidth at the -3 dB points is approximately 1 degree at 75 kHz, increasing to nearly 3.5 degrees at 10 kHz. In Fig. 4(c) and (d), the large peak to the left of the main lobe is the result of boats passing behind the testing area.

The operating feature of paramount importance in ADONIS is the shape of the beams. At the design stage, it was considered essential to predict the beam patterns accurately, in order to estimate imaging performance. The good agreement between theory and experiment in Fig. 4 provides confidence that the system does indeed perform as intended.

IV. TARGETS

Three different types of target were used in the imaging experiments: square, planar panels of area 1×1 m^2; cylindrical, polyethylene drums with a capacity of 113 l (30 U.S. gallons), 0.76 m high, 0.5 m in diameter, with a wall thickness of 0.5 cm; and a hollow, titanium sphere with a diameter of 70 cm and wall thickness of 1.5 cm. A swimming diver with a closed breathing system was also used as a target and, as reported elsewhere,[10] acoustic daylight images were obtained as he moved across the field of view.

The panels were mounted on 3×3 m^2 square frame resembling a tic-tac-toe board, which was placed vertically on the seabed (Fig. 5) in front of ADONIS at a range of 40 m. The face of the frame was approximately normal to the axis of the dish. Most of the panels were flat, and constructed of
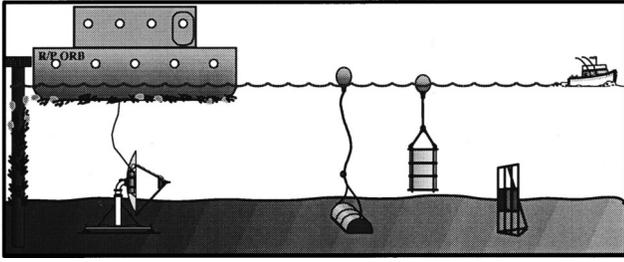
FIG. 5. Schematic of the ADONIS deployments below R. P. ORB. In practice, the various types of target illustrated in the figure were not deployed simultaneously. To the left of ORB is one of the pier pilings.

wood, fiberglass, aluminum, or aluminum faced with neoprene foam. One panel was of corrugated steel 3.2 mm thick..

The cylindrical drums were filled with wet sand (density ≈ 1900 kg/m^3), sea water (density ≈ 1000 kg/m^3), or syntactic foam (density ≈ 290 kg/m^3), referred to hereafter as the sand drum, the water drum, and the foam drum, respectively. Each drum was clamped with 6.4-mm-diam connecting rods between steel endplates, 6.4 mm thick, and weights were attached to the base of the foam drum to make it negatively buoyant. These drums were deployed in the water column, suspended from surface flotation units, and also partially submerged in the silty sediment forming the seabed (Fig. 5). In all cases the axis of each drum was perpendicular to the axis of the dish.

In a number of the water column deployments, several drums were suspended simultaneously from a 4-m-long floating wooden beam, an arrangement which allowed constant spacing between targets to be maintained. Both ends of the beam were anchored to fix orientation and distance from ADONIS. The depth of the targets was set so that at mid-tide the center of mass of each drum was 2 m above the seafloor, placing it in the middle of ADONIS' field of view. In the bottom deployments, divers arranged the drums at a range of approximately 15 m from ADONIS, which was tilted downwards by 10 degrees to keep the target in the field of view. From the point of view of imaging, these seabed deployments were particularly challenging, since the drums were partially (30%–50%) buried in the silty sediment.

The spherical target was supported in a metal cage, weighted to make it negatively buoyant, and suspended from surface floats (Fig. 5) at a depth of 2 m above the seafloor at mid-tide. As with the suspended drums, the sphere at mid-tide was then in the center of ADONIS' field of view.

V. DEPLOYMENT PROCEDURES

ADONIS was deployed through a moonpool in the rectangular, annular barge R. P. ORB, which was moored at the end of the Marine Facilities (MarFac) Pier, San Diego Bay. The water depth in this sheltered location is a nominal 7 m. Once it was in place on the seabed, the clearance between the top of the dish and the sea surface was about 3 m. Figure 5 shows the deployment configuration, with ADONIS beneath ORB looking towards the targets.

For many of the trials, a video camera was used to record conditions on the surface, particularly boat traffic and

swell. Beneath the surface, as a precautionary measure in the early experiments, a programmable, high-frequency acoustic source was mounted on the target frame. This source was activated intermittently (usually at the beginning and end of each data collection period) to confirm the alignment of the receiver with the targets. Thus, the source and hence the target positions within an image were localized to within one pixel. Incidentally, this same source was used for determining the in-water beam patterns of ADONIS.

As an additional check, the dish was periodically panned over the object space, causing the target to migrate back and forth across the image plane. This is an important test of the integrity of the imaging system, since it ensures that the target seen in an image is not an artifact associated with errors in calibration or equalization of the channels. Considerable attention was paid to balancing the 126 channels because the acoustic contrast in most acoustic daylight images is generally less than 4 dB, implying that even small errors in equalization could have resulted in false detection.

VI. AMBIENT NOISE SOURCES IN THE EXPERIMENTAL AREA

Within the calm, shallow waters of San Diego Bay, the three dominant sources of acoustic energy within the frequency range of ADONIS are snapping shrimp, industrial activity, and boat traffic. Marine mammals in pens several hundred meters distant from the experimental site also make a minor contribution to the background noise field, but this had little effect on the acoustic daylight experiments. Of the three main sources, the pulses from snapping shrimp feature most prominently in the time series of the noise. Several species of shrimp were collected near the experimental site, including *Synalpheus lockingtoni, Alpheus clamator*, the related genus *A. californiensis*, and *A. bellimanus*. Typically, these creatures are the size of a thumb nail, yet they are capable of producing extremely energetic, very brief pulses of sound with a broad bandwidth extending up to 200 kHz or beyond. Source levels may be as high as 190 dB *re* 1 μPa^2 at 1 m with a duration of the order of 5 μs or less.[14–16]

In general, snapping shrimp do not swim well, and they tend to cluster in colonies around pier pilings, outcrops of rock, kelp holdfasts, and similar habitats which offer the animals shelter.[17] No seasonal variations in shrimp activity have been reported, although a slight diurnal fluctuation in intensity is sometimes observed, with the shrimp noise marginally louder at dawn and dusk.[18] On the basis of these observations, we expected the noise created by snapping shrimp during the ORB imaging experiments to originate from fixed directions and to be more or less continuous throughout the day and night. The evidence from our observations with ADONIS is consistent with this picture of the shrimp noise.

Industrial noise in the experimental area also exhibits a fixed spatial pattern, but shows strong diurnal fluctuations which correlate with human activities around the shoreline. The noise produced by dockside machinery and shore activity generally contains more lower frequency acoustic energy than the pulses from the snapping shrimp. This was exemplified in some of the early ORB experiments, when the targets were inadvertently aligned with a naval loading dock
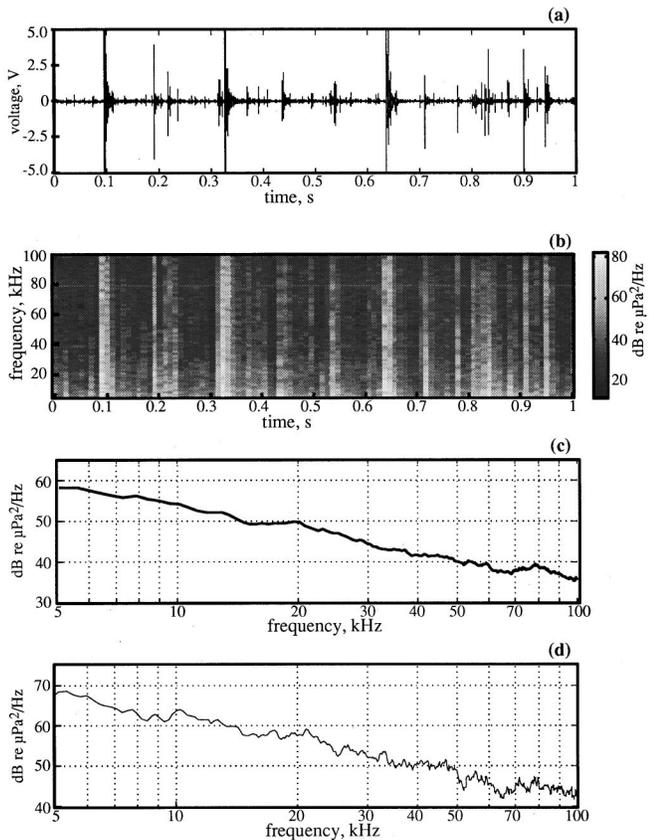
FIG. 6. (a) One second time series of (omnidirectional) ambient noise showing snapping shrimp pulses. (b) Spectrogram of the time series in (a) with the gray scale representing power spectral density. (c) Power spectral density of the noise, averaged over 30 s. (d) Power spectral density averaged over 15 shrimp pulses.
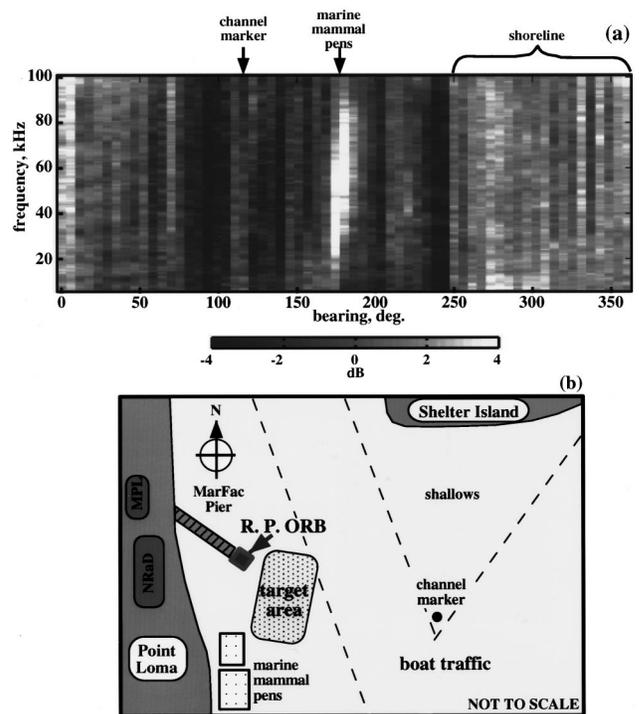

FIG. 7. (a) Frequency-azimuth plot of the noise, obtained by rotating ADONIS through 360 degrees in the horizontal. In a given frequency cell, the data are referenced to the noise level averaged over all bearing angles. (b) Plan view of the experimental site showing the test area and local features that affected the ambient noise environment.

across the bay. Occasionally, the low-frequency noise generated around the dock area was more intense than the scattered noise from the targets, with the result that the targets appeared in silhouette at the lower frequencies in the acoustic daylight images.

Shipping and surface traffic produce a broad spectrum of sound, extending from below 100 Hz up to several kHz.[19] At the lower frequencies, tonals appear associated with shaft and propeller blade rates, while cavitation produces a continuous spectrum extending to the higher frequencies. As a ship's speed increases, the radiated noise levels rise, implying that sound from vessels sufficiently close to the targets, such that the higher frequencies are not significantly attenuated, will contribute to the imaging process. Unlike shrimp and industrial noise, the component of the noise field generated by surface traffic shows a highly variable directionality. Accordingly, during daylight hours, when a high density of recreational and naval traffic is present, the ambient noise field in San Diego Bay is very variable, especially towards the lower end of the frequency band used for acoustic daylight imaging.

Examples of the omni-directional, broadband noise data collected with a low-self-noise hydrophone mounted on the rim of the ADONIS reflector (outside the focal region) are shown in Fig. 6. The data were recorded during late evening hours, when little boat or industrial noise was present. Figure

6(a) shows a 1 s time series in which the noise is dominated by brief, energetic bursts of sound from local snapping shrimp. Counting only those pulses whose amplitude exceeds 10% of the highest peak level, the average period between snaps is 30 ms, which provides a useful measure of the averaging time required to obtain a temporally stable acoustic daylight image with this type of ensonifying field. Incidentally, the width of the pulses in Fig. 6(a) is about 8 μs, which is actually the temporal resolution of the system, rather than the true width of a snapping shrimp pulse.

Figure 6(b) shows a spectrogram of the time series in Fig. 6(a), in which each vertical stripe represents an average power spectrum computed from 12 individual spectra obtained from 10 ms of data, with 70% overlap, using 512-point FFTs. It is clear from a casual comparison of the time series with the spectrogram that the pulses exhibit a broad spectrum extending up to at least 100 kHz, which is approximately the bandwidth of the measurement system. Note that the noise power varies by as much as 65 dB over a time scale as brief as 10 ms.

The spectrum of a longer time series is shown in Fig. 6(c). In this case, the data were split into 30 1-s segments, each of which was Fourier transformed in a standard way: Hanning windowing, 2048-point FFTs with 50% overlap, providing 220 spectra in the 1-s average. All 30 of the resultant spectra were then further averaged to obtain the spectrum in Fig. 6(c), which has a spectral resolution of approximately 100 Hz. The spectral gradient is −18.5 dB/decade, which is slightly steeper than the slope of wind-generated noise from breaking waves.[20]
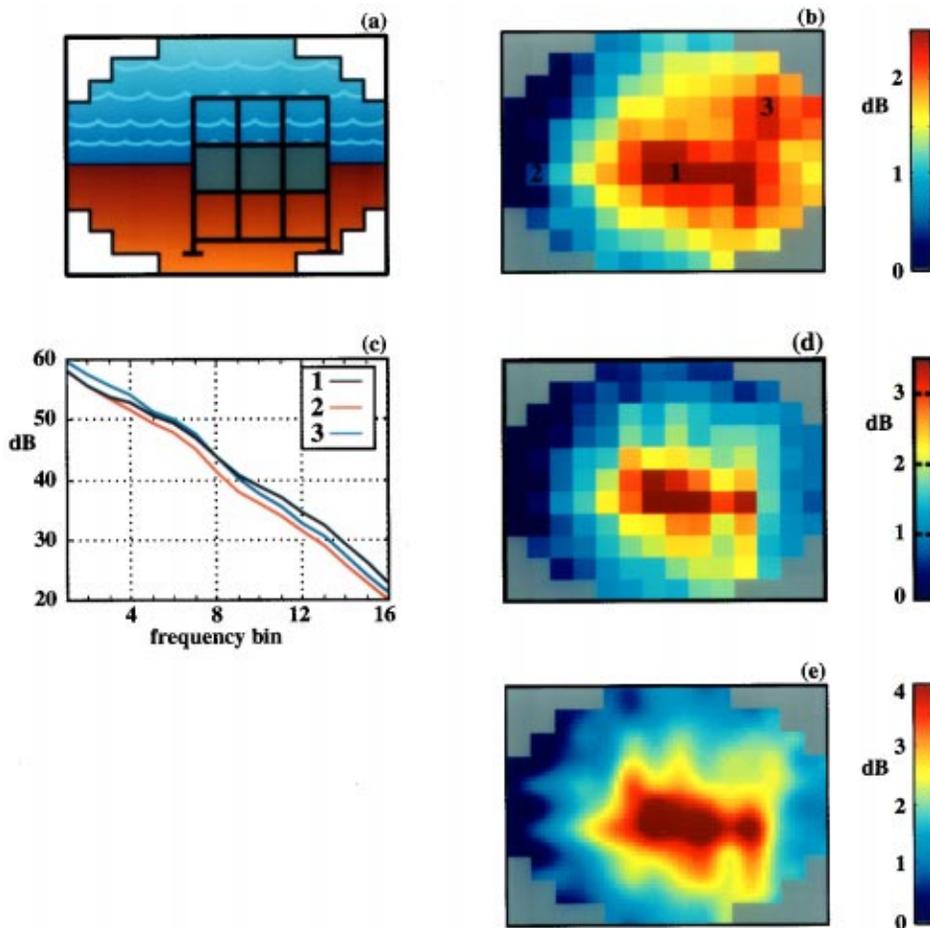
FIG. 8. Bar target at a range of 38 m. (a) Schematic of the scene falling within the field of view of ADONIS. (b) Uninterpolated, broadband, intensity mapped image formed by linearly averaging data from all sixteen frequency bins (8.5 to 75 kHz). (c) Spectrum of the noise in pixels on-target in dB re 1 μPa^2/Hz. (1), left of target (2), and above target (3). (d) Uninterpolated intensity mapped image formed by averaging over the top three frequency bins (57 to 75 kHz). (e) Interpolated version of the image in (d). The images in (b), (d), and (e) were formed from data taken at the same time.

To investigate the spectral content of the snapping shrimp pulses, 15 of the more energetic events were selected from the time series, Fourier analyzed, and averaged. The resultant spectrum is shown in Fig. 6(c). On comparison with the spectrum of the continuous time series in Fig. 6(c), it can be seen that, although the level of the shrimp spectrum is higher by about 8 dB, the spectral gradient is the same: -18.5 dB/decade. Although not conclusive, this observation suggests that the overwhelming contribution to the spectrum of the long time series in Fig. 6(c) is energy from the snapping shrimp pulses.

VII. HORIZONTAL ANISOTROPY OF THE NOISE

By rotating ADONIS in the horizontal using the hydraulic motor mounted within the mast, it was possible to measure the azimuthal dependence of the noise field through a full 360 degrees. A low-self-noise hydrophone mounted to the right of the imaging array, but within the focal region, was used to acquire the noise data. The beam pattern of this phone was horizontal, with essentially the same shape as that of the receivers in the main array head. Figure 7(a) shows the spectral and angular dependence of the noise, as observed in the early hours of the morning when no boats were present. The data set spans 10 min, with each vertical stripe computed from 10-s segments of the time series, corresponding to an angular scan of 5.5 degrees. Each segment was Fourier analyzed with 2048-point FFTs applied to time-windows

with 50% overlap, providing 2200 terms in the average and a spectral resolution of approximately 100 Hz. The spectra were then normalized by the average spectrum taken over the 360 degree scan.

The azimuthal variation of the noise spectral density in Fig. 7(a) amounts to about 8 dB. To interpret the origin of the anisotropy, the spectrogram may be compared with the plan view of the area around the experimental site in Fig. 7(b). A prominent feature in the spectrogram is the high energy burst around 180 degrees, which aligns with the marine mammal pens, and is attributed primarily to dolphin vocalizations. Between 250 and 360 degrees is a broad swath of noise, which arises mainly from snapping shrimp inhabiting the pier pilings and rocks along the shore. The noise signature at 110 degrees is also due to snapping shrimp, in this case a colony occupying the channel marker piling close to Shelter Island.

It is apparent from Figs. 6 and 7 that the ambient noise field around the MarFac Pier in San Diego Bay is highly variable, azimuthally nonuniform, and dominated by snapping shrimp noise. As far as acoustic daylight imaging is concerned, the shrimp noise provides excellent ensonification because of its broad bandwidth and high source level. Much of the shrimp noise originates on the pier behind ADONIS, giving rise to front ensonification of the targets. Any additional noise from passing vessels will also affect the imaging, in a way that depends on range and bearing. As the boats are mostly confined to channels in front of ADONIS,
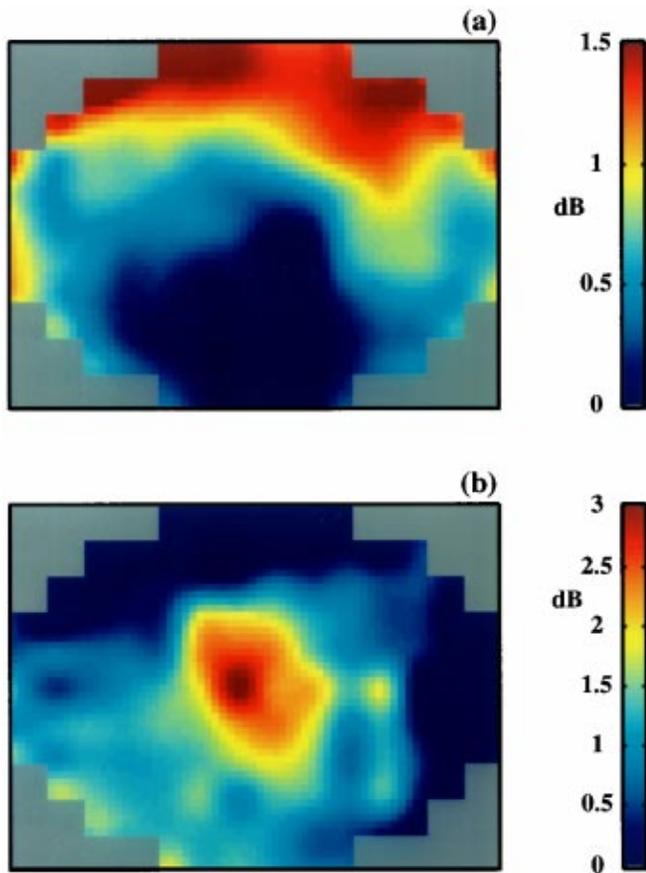
FIG. 9. Interpolated, intensity mapped images of the bar target at a range of 38 m. The two images were formed from data taken at the same time. (a) Low-frequency silhouette, formed by averaging over frequency bins 2, 3, and 4 (10 to 13.8 kHz). (b) High-frequency, front-ensonified image, formed by averaging over frequency bins 14, 15, and 16 (57 to 75 kHz).

their contribution to the noise field often increases the intensity of the noise from behind the target, tending to create a silhouette effect.

If snapping shrimp noise were unique to the San Diego area, then its utility in connection with acoustic daylight imaging would be limited, but it appears that this is not the case. The available evidence indicates that snapping shrimp are ubiquitous in temperate and tropical coastal waters, wherever appropriate habitats exist.[15,21–24]

VIII. IMAGE FORMATION BY INTENSITY MAPPING

To create the acoustic daylight images, the intensity in each beam is mapped into a corresponding pixel on the screen of a computer monitor. Each image is rectangular, containing 14×11 pixels, with those pixels in the corners containing no information since there are no receivers at these locations. Thus, the useful image is approximately elliptical, having the same shape as the hydrophone array at the focal surface of the dish. The pixels show color, produced from the "jet" colormap, with blue and red, respectively, representing low and high acoustic intensity over a band of frequencies. (In a few images, intensity mapping is not used but instead color represents the intensity at different frequencies, that is to say, "acoustic color.") In all the in-

tensity mapped images presented below, the acoustic contrast between pixels is referenced, in dB, to the lowest intensity pixel.

The raw data from ADONIS yields images that are rather coarse grained, which often makes it difficult to recognize a target. A significant improvement in image quality is achieved by interpolating between data points. The interpolation algorithm used is a bi-cubic, by a factor of 5 in each direction. This inserts four additional points between each pair of original data points, resulting in a new 51×66 image matrix instead of the original 14×11.

The intermittent character of the snapping shrimp noise [Fig. 6(a)] leads to a strong frame-to-frame variation in image intensity. The fluctuations are very evident in the sequences of moving images in which the screen is refreshed once every 40 ms. To alleviate the problem, time averaging is performed over a certain number of frames. In the moving sequences, either boxcar or exponential averaging is used, to provide a running average over a number of previous frames. Boxcar averaging is used to produce the still images. The time averaging, performed over 10 s (i.e., 250 frames) in all the images presented below (except in Fig. 15) stabilizes the images significantly.

Since the intensities at each frequency are estimated sequentially, the time window for each frequency bin within a frame is only 1.5 ms, with a period of 40 ms separating successive estimates in the same frequency bin. Thus, for 250 frames, the total window time for any particular bin is only 375 ms, or less than 4% of the total averaging time of 10 s. According to Fig. 6(a), there are on average 33 recognizable snapping shrimp pulses per second, with each pulse sufficiently brief to fall completely within the time window of a frequency bin. On average, only 13 of these pulses will occupy a given frequency bin in the 10-s interval over which the averaging was performed. One way of increasing the number of shrimp pulses contributing to an image is to average over several frequency bins, which is the approach adopted here. By averaging over three neighboring frequency bins, the effective windowing time is extended from 0.375 to 1.13 s, corresponding to 12% of the collected data.

In the moving sequences and most of the stills, the images are normalized by dividing the intensity in each pixel by the average intensity in all the pixels. This procedure leads to some improvement in frame-to-frame stability, but generally the effect is less pronounced than that due to time averaging.

IX. IMAGES OF THE PLANAR TARGETS

A. The horizontal bar

Figure 8 shows acoustic daylight images of a rectangular target formed from three square aluminum panels each 3.2 mm thick and faced with closed-cell neoprene foam 6.4 mm thick. The foam side of the panels faced towards ADONIS and the range to the target was 38 m. The scene within the field of view of ADONIS is illustrated in Fig. 8(a). In Fig. 8(b), a raw (uninterpolated) broadband image is shown, formed by averaging all sixteen frequency bins (8.5 to 75 kHz) over 250 frames, corresponding to 10 s of data. At the
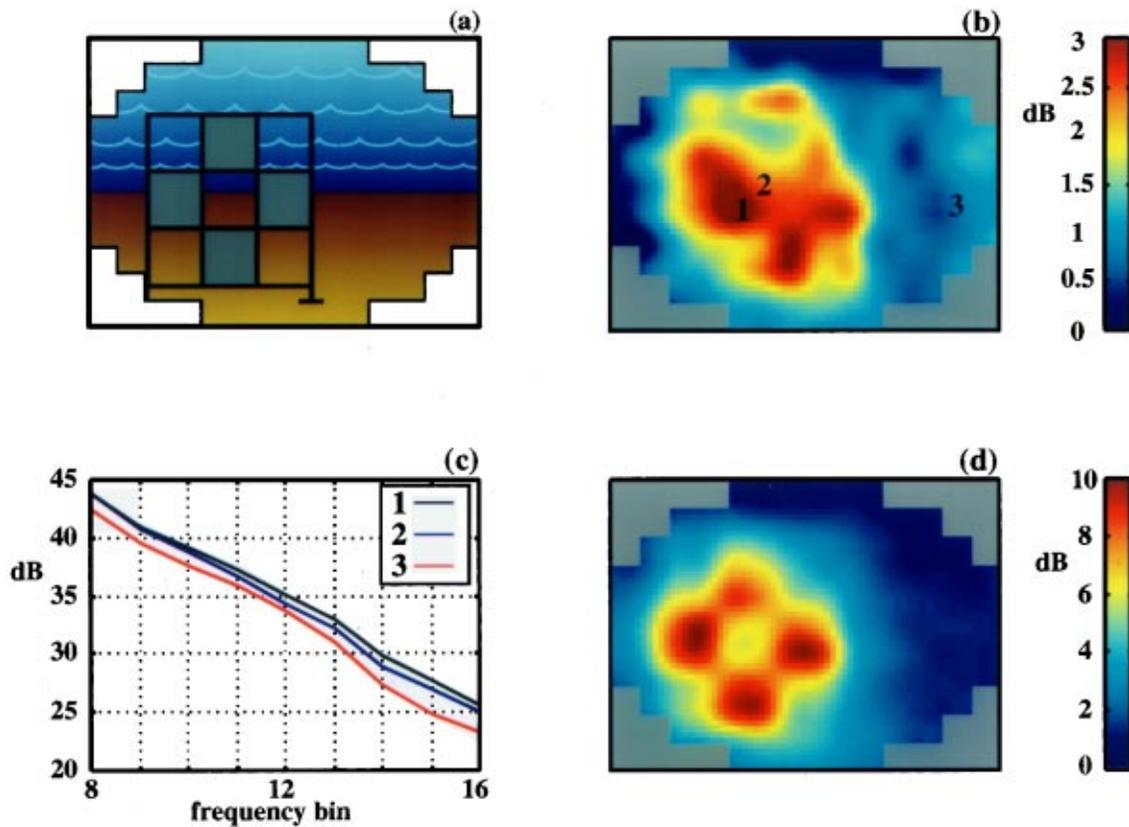
FIG. 10. The fenestrated cross at a range of 38 m. (a) Schematic of the scene falling within the field of view of ADONIS. (b) Example of a poor quality, high-frequency interpolated, intensity mapped image formed by averaging data over the top three frequency bins (57 to 75 kHz). (c) Spectrum, in dB re 1 μPa^2/Hz, of the noise in pixels, as identified in (b), on a target panel (1), in the central window (2), and off the target (3). (d) Example of a good quality, high-frequency, interpolated, intensity mapped image formed by averaging data from the top three frequency bins (57 to 75 kHz).

highest frequency, the beamwidth of 0.75 degrees gives an areal coverage of approximately 0.5×0.5 m^2 at the target range, or in other words four beams intersect each 1×1 m^2 target panel. The noise spectra in three pixels, one on and the other two off the target, are illustrated in Fig. 8(c), where it can be seen that the acoustic contrast, represented by the difference between the curves, tends to increase with increasing frequency. Figure 8(d) shows another raw image, formed in this case from an average of the top three frequency bins (57 to 75 kHz). The improvement in resolution obtained at the higher frequencies is quite evident on comparing Fig. 8(b) and (d). When interpolation is applied to the data in Fig. 8(d), the image in Fig. 8(e) is obtained. At these higher frequencies, the target is front ensonified from snapping shrimp on the pier pilings.

Although the target is visible in the raw, broadband data shown in Fig. 8(b), the low resolution resulting from the lower frequencies, combined with the granular pixel structure, give rise to a rather poor quality image. A distinct improvement in resolution can be seen in Fig. 8(d), where the low frequencies have been removed. Visually, the smoothing introduced by interpolation leads to a further improvement in image quality, as evident in Fig. 8(e), where the elongated shape of the bar is recognizable.

As the directionality of noise varies, for whatever reason, the appearance of the images changes accordingly. Thus, there is no typical acoustic daylight image of a particular target, in the same way that there is no typical photograph of a given scene in daylight. In both cases, front and back illumination, for example, create different shadowing structures and hence different visual effects. The point is well illustrated by the low- and high-frequency, interpolated images of the bar target shown in Fig. 9. The low-frequency image in Fig. 9 is an admittedly crude silhouette, formed by back ensonification from the naval loading dock on the far side of San Diego Harbor. In the higher-frequency image the bar is front ensonified, probably from local snapping shrimp on the MarFac Pier pilings. Although the images in Fig. 9 are both of rather poor quality, the low-frequency silhouette can be seen to align with the high-frequency front-lit image of the bar. It is interesting that the effect seen in these two images is rarely observed in photography, namely, front illumination in one spectral band and, simultaneously, back illumination in another.

B. The fenestrated cross

Figure 10 shows another planar target, in the form of a fenestrated cross [Fig. 10(a)]. The panels, aluminum faced with neoprene foam, were the same as those forming the bar target in Fig. 8. Again, the range was 38 m and the foam side of the panels was facing ADONIS. At the time of the deploy-
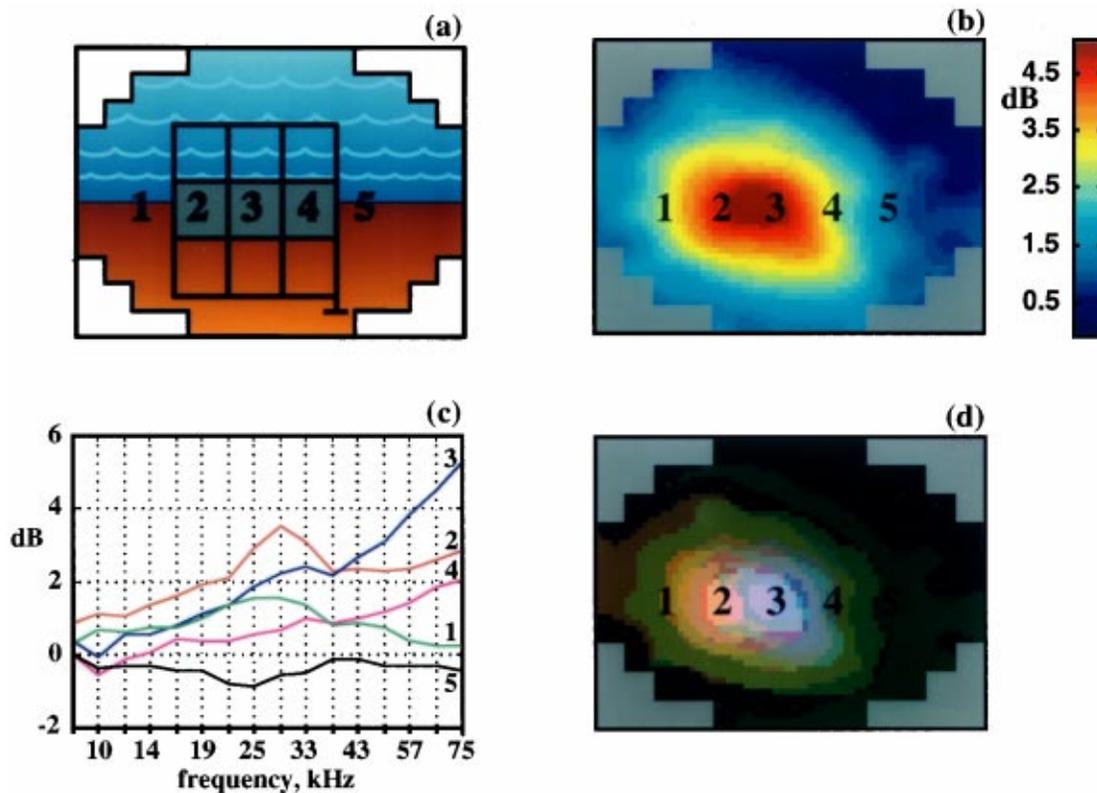
FIG. 11. Three metal panel targets at a range of 40 m. (a) Schematic of the scene falling within the field of view of ADONIS. Panel (2) on the left is 3.2-mm-thick aluminum faced with 6.4-mm-thick neoprene foam, with the metal side facing ADONIS. In the center, panel (3) is of 6.4-mm-thick aluminum. At the right, panel (4) is of 3.2-mm-thick corrugated steel. (b) Intensity mapped, interpolated image averaged over frequencies 24.6 to 75 kHz. (c) Selected spectra from pixels in (b), normalized to the image average. (d) RGB interpolated image formed from the same data as in (b) but with low frequencies mapped into red, middle frequencies into green and high frequencies into blue.

ment it was uncertain whether the central window would be resolved because, at the highest frequency of 75 kHz, the window was just within the limits of resolution of ADONIS (four beams fall within the window). However, the window has been resolved, although the quality of the image varies from frame to frame due to the variability of the ensonifying noise field. Figure 10(b) and (d), respectively, shows examples of a poor- and a high-quality interpolated image, averaged over the top three frequency bins (57 to 75 kHz) in both cases. Note that in Fig. 10(d), the contrast between the panels and the background is about 10 dB, which is significantly higher than expected based on the anisotropy of the noise field that usually prevailed in the area. This was one of the first deployments of ADONIS for which little environmental information is available, but it is known that at around the time the data were taken an extremely noisy angle grinder was being used on the MarFac Pier. The grinder would have provided very strong frontal ensonification, which is consistent with the high contrast in the image.

Even in the case of the poorer quality image [Fig. 10(b)] the central window is just distinguishable, and the contrast across the image is in the region of 3.5 dB. Three spectra from this image are shown in Fig. 10(c), one from a pixel on a panel, one from the background, and the third from the central window. By comparison, the window in the high-quality image [Fig. 10(d)] is clearly resolved and easy to distinguish.

Figure 11 shows a bar target [Fig. 11(a)] formed from three square panels made of different materials, placed at a range of 40 m. The left panel (labeled 2) was 3.2-mm-thick aluminum sheet faced with 6.4-mm-thick neoprene foam, with the metal side facing ADONIS. In the center (labeled 3) was a 6.4-mm-thick aluminum sheet; and on the right (labeled 4) a 3.2-mm-thick steel corrugated panel of the type often used on sheds and storage buildings. In this deployment the target frame had been moved by approximately 10 degrees to the left of its original position, to avoid back ensonification from the naval loading dock on the far side of the bay.

Figure 11(b) shows an intensity-mapped image averaged over frequency bins 8 to 16 (24.6 to 75 kHz). The metal and foam panel (2) and the metal panel (3) are clearly visible with a contrast around 4.5 dB, while the corrugated panel (4) shows up but with a lesser contrast of 2.5 dB. However, the spectral content of all three panels differs, as can be seen in Fig. 11(c). At the lower frequencies, below 37.5 kHz, panel (2) is the best scatterer of acoustic energy, at higher frequencies panel (3) dominates, and across the full spectral range the corrugated panel (4) is less efficient at scattering than either of the other two panels.

C. RGB mapping

To utilize the spectral differences between the panels, different frequencies may be mapped into separate color components in the image. In this type of representation, the
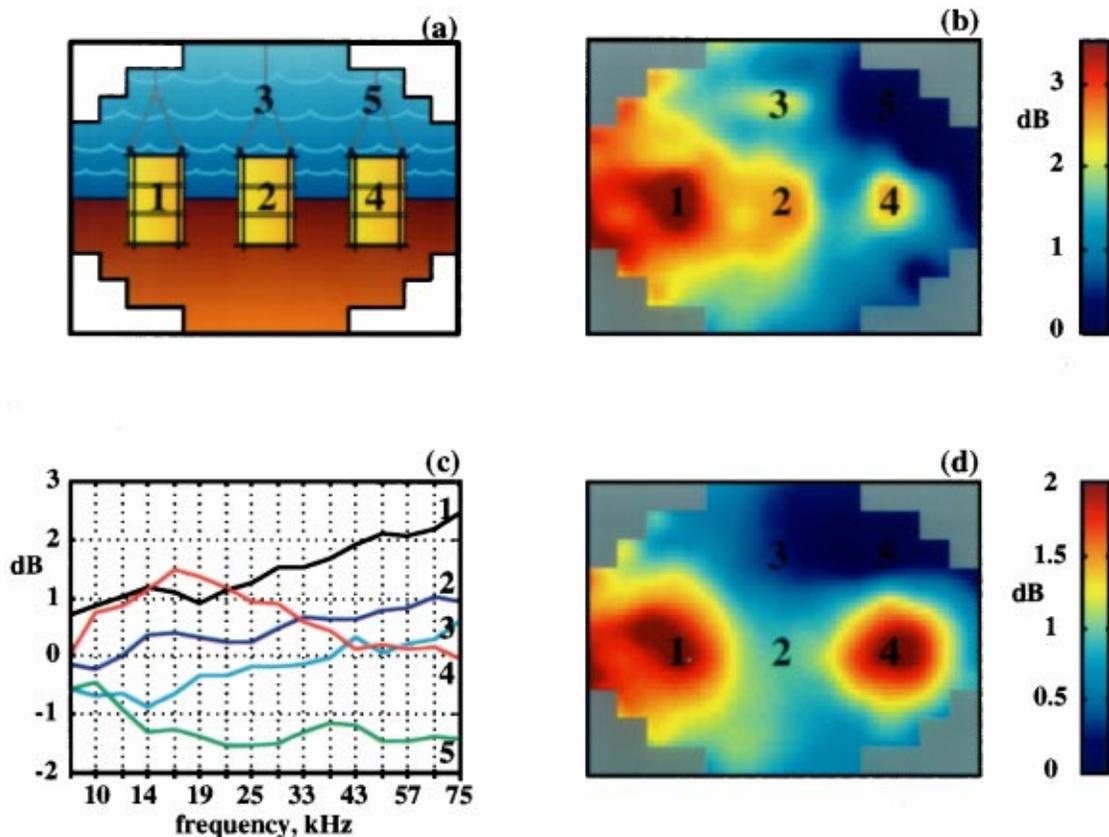
FIG. 12. Suspended drum targets at a range of 20 m. (a) Schematic of the scene falling within the field of view of ADONIS. Left, foam drum (1), center, water drum (2), and right, sand drum (4). (b) High-frequency, intensity mapped, interpolated image formed by averaging over the top three frequency bins (57 to 75 kHz). (c) Selected spectra of pixels in the image, normalized to the image average. (d) Low-frequency, intensity mapped image formed from the same data, averaged over frequencies 10 to 13.8 kHz.

hue and saturation are an indication of frequency content and the luminosity is an indicator of overall intensity. Thus, this type of imaging incorporates frequency and intensity information and the resultant ''acoustic color'' in the image can be exploited to discriminate between targets of similar shape but differing composition.

To generate Fig. 11(d) the frequency band was divided into three equal parts, with the lower range mapped into red, the middle into green, and the top into blue. Visually, it can be seen in this RGB image that the color of the panels changes from reddish-pink on panel (2), to light pinkish-blue on panel (3), to dark greenish-blue on panel (4). Thus, all three panels can be distinguished from one another simply from their different coloration.

Intensity mapping [Fig. 11(b)] and RGB mapping [Fig. 11(d)] in combination provide extensive information about the composition of the object being imaged. It follows that these mappings show promise for classifying targets. However, much needs to be learned about the acoustic scattering properties of various targets and target materials before the classification potential of the mapping schemes can be fully exploited.

X. IMAGES OF THE CYLINDRICAL TARGETS

A. Drums in the water column

The panel targets discussed above presented a large surface area normal to the axis of the ADONIS dish, making

them relatively easy to image, particularly when front ensonified by the snapping shrimp on the MarFac Pier. Because of their curvature, the cylindrical targets were more challenging, since they presented only a narrow vertical stripe normal to the axis of the dish. Three polyethylene drums were used in the experiments, one filled with syntactic foam (essentially air), a second with seawater, and the third with wet sand.

Figure 12 shows two examples of intensity-mapped, interpolated images obtained when the drums were suspended from the sea surface [Fig. 12(a)] at a horizontal range of 20 m. From left to right the drums contain foam, water, and sand. The high-frequency image in Fig. 12(b) was averaged over the top three frequency bins (57 to 75 kHz), and the lower-frequency image in Fig. 12(d) was averaged over bins 2 to 4 (10 to 13.8 kHz).

In the high-frequency image of Fig. 12(b), all three drums are visible with acoustic contrasts of approximately 4 dB (foam) and 2.5 dB (both water and sand). Additionally, the supporting shackle is visible above the water drum. The picture is different at the lower frequencies [Fig. 12(d)], where the foam and sand drums show a contrast of 2 dB, while the water drum and shackle are not visible at all. These visual features in the two images are consistent with the spectra shown in Fig. 12(c).

Perhaps the most interesting question concerning Fig. 12 is why the water drum is visible in the high-frequency image, given that its acoustic impedance was much the same as that
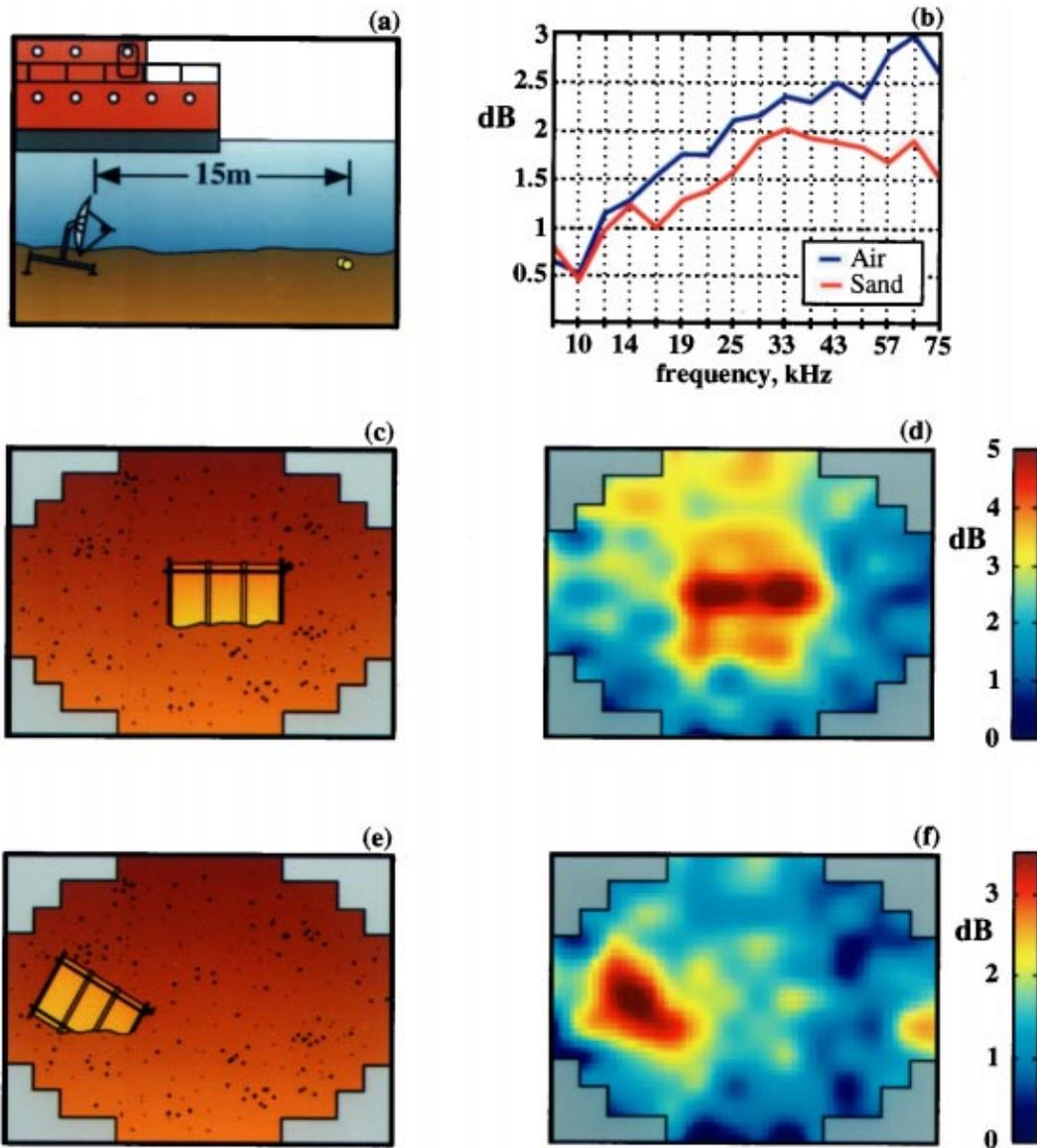
FIG. 13. Drums on the seabed at a range of approximately 15 m. (a) Experimental arrangement, showing ADONIS tilted forward by 10 degrees to point towards the bottom. (b) Spectra of pixels on the foam and sand drums, normalized to the image average. (c) Schematic of ADONIS' view of the foam drum. (d) Intensity mapped, interpolated image of the foam drum, formed by averaging over the top three frequency bins (57 to 75 kHz). (e) Schematic of ADONIS' view of the sand drum. (f) Intensity mapped, interpolated image of the sand drum, formed by averaging over the top three frequency bins (57 to 75 kHz). Note that in the image the axis can be seen to be tilted by approximately 45 degrees.

of the background water. The answer to this may lie in the way the drums were deployed. The sand drum was negatively buoyant by at least 135 kg and the foam drum was weighted to be negatively buoyant by 55 kg. The water drum, however, was weighted only with the 10 kg of its supporting cage. In a series of images created with shorter averaging times, the water drum can be seen to sway back and forth, a movement which causes the rusty metal components of the shackle and drum cage to rub together and generate noise. Spectra 2 and 3 in Fig. 12(c) are similar in shape, consistent with both being generated by the same mechanism. Moreover, the noise from the water drum and shackle was observed to rise when large boat wakes passed over the targets, while the noise from the foam and sand drums remained essentially unchanged. Based on this evidence, it seems that the water drum and shackle are visible in the

high-frequency image through their own self-noise rather than through scattering of the ambient noise field.

B. Drums on the bottom

To investigate the imaging performance of ADONIS against targets on the seabed, the foam and sand drums were held horizontally and dropped from the surface onto the bottom at ranges of 13 m and 15 m, respectively, from the dish. ADONIS was tilted forward by 10 degrees [Fig. 13(a)] so the drums would be in the center of the field of view. On impact, the drums became partially buried in the soft mud bottom, with 30%–50% of their volume below the interface. The sand drum landed slightly askew, with its axis angled down into the mud at approximately 45 degrees [Fig. 13(e)]. The axis of the foam drum was essentially horizontal [Fig. 13(c)],
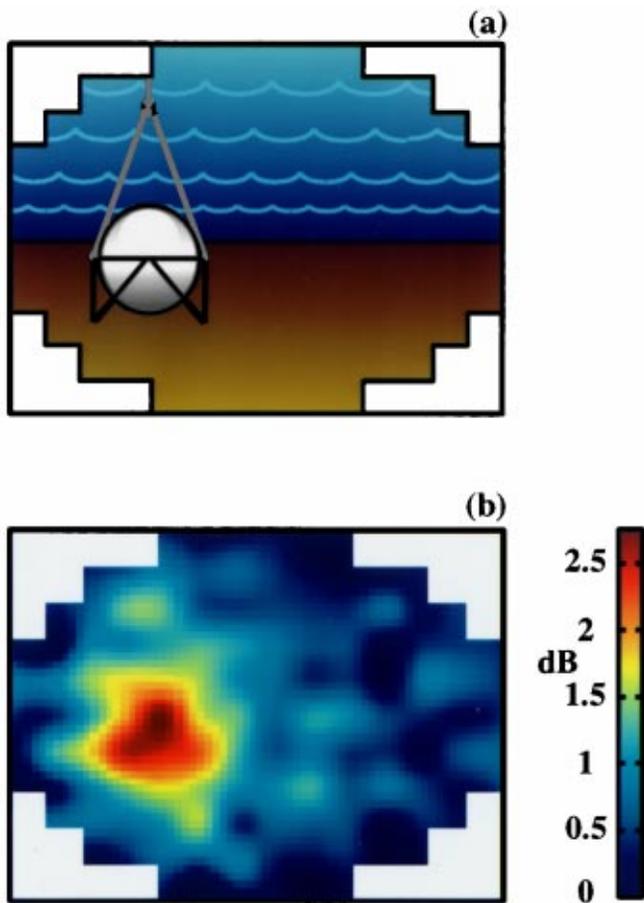
FIG. 14. Spherical titanium shell at a range of 25 m. (a) Schematic of the scene falling within the field of view of ADONIS. (b) Intensity mapped, interpolated image formed by averaging over the top three frequency bins (57 to 75 kHz).

and in both cases the axes were perpendicular to the axis of the dish.

The acoustic daylight image of the foam drum, formed from an average of the top three frequency bins (57 to 75 kHz), is shown in Fig. 13(d). Although the background is now the sediment, the acoustic contrast in the image is approximately 4 dB, which is essentially the same as when the drum was suspended in the water column [Fig. 12(b)]. An image of the sand drum, also averaged over the top three frequencies, is shown in Fig. 13(f). The contrast in this case is approximately 3 dB, which is similar to the contrast observed when the drum was suspended in the water column. By comparing Fig. 13(d) and (f), it is apparent from the images that the axis of the foam drum is horizontal and that of the sand drum is tilted at about 45 degrees. Figure 13(b) shows the normalized spectra of pixels on each of the bottom deployed drums. These spectra show much the same trends as those of the suspended drums in Fig. 12(c), which is consistent with the similar contrast in the images of the drums on the bottom and in the water column.

XI. IMAGING THE SPHERICAL TARGET

Geometrically, the titanium sphere represents a more challenging target than either the planar panels or the cylin-

drical drums. With a surface showing curvature in two orthogonal directions, the sphere presents only a small, spot-like area of surface normal to the axis of ADONIS, compared with a stripe in the case of the drums and a square for each of the panels. This difficulty is offset by the fact that the sphere is actually an air-filled shell with an acoustic impedance significantly different from that of water. Like the foam drum, it may therefore be expected to act as a good target for acoustic daylight imaging. As with the drums, the sphere was suspended from surface floats at a horizontal range of 25 m from the dish [Fig. 14(a)]. Deployment ropes were tied directly to the cage supporting the sphere, avoiding the use of a shackle, to alleviate the problem of self-noise in the system.

Figure 14(b) shows the interpolated acoustic daylight image of the sphere formed by averaging the top three frequency bins (57 to 75 kHz). The equator and upper hemisphere are clearly visible in the image, with a maximum contrast close to 2.5 dB. Below the equator, the lower hemisphere is difficult to distinguish, indicating that any energy scattered from this region must be several dB less than that from the upper hemisphere. In several respects, this image resembles Potter's[5] numerical simulation of a sphere ensonified by surface sources in shallow water.

At the time the data for Fig. 14 were collected, however, the surface was calm and there were few surface sources. Most of the noise was generated by snapping shrimp on the pilings of the MarFac Pier, which provided horizontal, front ensonification. This raises the question as to why the top hemisphere and the equator should show a significantly stronger contrast than the lower portion of the sphere. One possibility is that the incident, horizontally traveling sound was deflected upwards and downwards by the upper and lower hemispheres, respectively. The upward deflected sound then encountered the highly reflective sea surface at near normal incidence, turned around and re-ensonified the top of the sphere, where it was scattered a second time, back towards ADONIS, to yield the high contrast in the image. The downward deflected sound behaved similarly except that it was reflected from the heavily attenuating bottom, a fine silty mud. There was, therefore, little energy available to ensonify the lower hemisphere from below and the acoustic contrast in this region of the image is correspondingly reduced.

As a consequence of the highly variable nature of the snapping shrimp noise (Fig. 6), successive frames, which are separated by intervals of only 40 ms, in general show significant variations in intensity. This is illustrated in Fig. 15, where a sequence of 12 successive frames of the spherical target is shown, with no temporal averaging. The sequence of frames was created from the top frequency, bin 16 (75 kHz), of the first 0.5 s of data used to form the image in Fig. 14(b). The sphere is difficult to identify in most of the images because of the high dynamic range of 20 dB, although it does stand out clearly in frame 10. Epifanio[10] presents further sequences of images, which indicate that at least 1 in 25 frames contains a bright spot associated with a target (see Fig. 7.18 in Ref. 10); he also discusses the effect of averaging times on image quality.
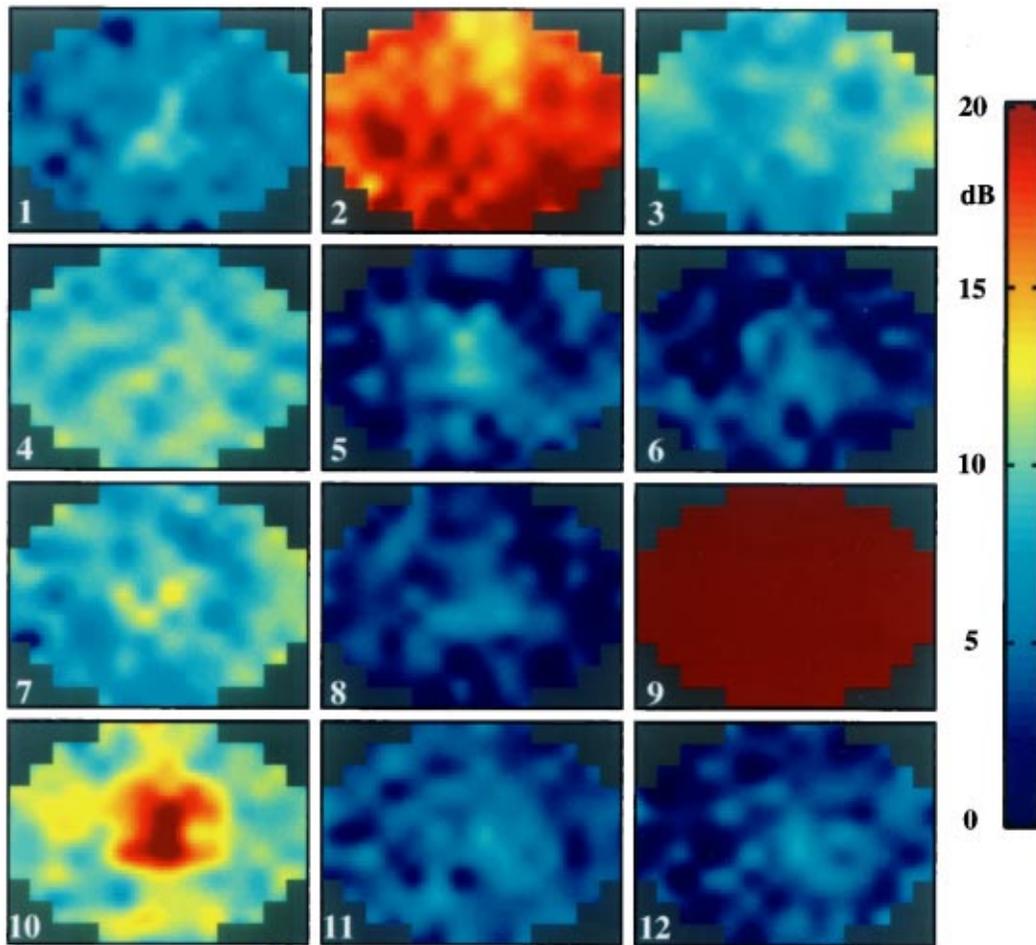
FIG. 15. Sequence of successive, intensity mapped interpolated images of the titanium sphere, formed from the top frequency bin 16 (75 kHz). The duration of this sequence of frames is approximately 0.5 s.

XII. CONCLUDING REMARKS

The images in this article are the first to have been obtained of objects in the ocean using naturally generated sound as the ensonification. In these early ORB experiments, the imaging system (ADONIS) was deployed close to shore in San Diego Bay, at the end of the MarFac Pier, and the principal source of noise was snapping shrimp inhabiting the pier pilings. A casual examination of the images reveals that the resolution falls far short of optical imaging, simply because of the limited aperture of the acoustic reflector used in the experiments: the pupil of the human eye is about 20 000 optical wavelengths across, whereas the diameter of the ADONIS dish is only 150 acoustic wavelengths at the highest operating frequency. Nevertheless, the images are recognizable in most cases, especially at the higher frequencies where the angular resolution is reasonable (approximately 0.6 m at a range of 50 m).

As with conventional photography, the appearance of a given scene in an acoustic daylight image shows considerable variability, depending particularly on the anisotropy of the ambient noise field at the time the data were collected. In other words, the shadowing in the images depends strongly on the directionality of the ensonification. During the experiments, as much environmental information as possible was recorded, including a measure of the horizontal directionality

of the noise. It was not feasible, however, to measure the horizontal anisotropy of the noise every time that imaging data were taken, making interpretation of some of the detailed, shadowing features in the images uncertain. However, considerable care was taken over the alignment of the ADONIS receiver and the targets, and checks were performed repeatedly to ensure that regions of enhanced contrast in the images are not artifacts of the system. The essential conclusion is that the acoustic daylight images obtained in the ORB experiments are genuine representations of the object space within the field of view of ADONIS.

ACKNOWLEDGMENTS

[1] S. Flatté and W. Munk, ''Submarine detection: Acoustic contrast versus acoustic glow,'' Report number JSR-85-108, MITRE Corporation, McLean, Virginia (1985).

[2] M. J. Buckingham, ''Ambient noise as a source of acoustic illumination in the ocean,'' Technical memorandum (April 1987). (Accepted by the United States Patent and Trademark Office, Serial No. 08/012,894, February 3, 1993 in support of Patent Number 5,333,129 on Acoustic Imaging in the Ocean using Ambient Noise, assigned July 26, 1994 to the Regents of the University of California, inventor, Michael J. Buckingham.)

[3] M. J. Buckingham, B. V. Berkhout, and S. A. L. Glegg, ''Imaging the ocean with ambient noise,'' Nature (London) **356**, 327–329 (1992).

[4] M. J. Buckingham, ''Theory of acoustic imaging in the ocean with ambient noise,'' J. Comput. Acoust. **1**, 117–140 (1993).

[5] J. R. Potter, ''Acoustic imaging using ambient noise: Some theory and simulation results,'' J. Acoust. Soc. Am. **95**, 21–33 (1994).

[6] B. D. Steinberg and H. M. Subbaram, *Microwave Imaging Techniques* (Wiley, New York, 1991).

[7] N. C. Makris, F. Ingenito, and W. A. Kuperman, ''Detection of a submerged object insonified by surface noise in an ocean waveguide,'' J. Acoust. Soc. Am. **96**, 1703–1724 (1994).

[8] M. J. Buckingham and J. R. Potter, ''Acoustic daylight imaging: vision in the ocean,'' GSA Today **4**(4) (1994).

[9] M. J. Buckingham, J. R. Potter, and C. L. Epifanio, ''Seeing underwater with background noise,'' Sci. Am. **274**, 86–90 (1996).

[10] C. L. Epifanio, ''Acoustic Daylight: Passive Acoustic Imaging using Ambient Noise,'' Ph.D. thesis, Scripps Institution of Oceanography, University of California, San Diego, 1997.

[11] R. H. Mellen, ''The thermal-noise limit in the detection of underwater acoustic signals,'' J. Acoust. Soc. Am. **24**, 478–480 (1952).

[12] H. B. Callen and T. A. Welton, ''Irreversibility and generalized noise,'' Phys. Rev. **83**, 34–40 (1951).

[13] G. B. Deane, ''The beam forming properties of a concave spherical reflector with an on axis receiver,'' J. Acoust. Soc. Am. **106**, 1255–1261 (1999).

[14] A. L. Anderson, ''Ambient-noise measurements at 30, 90, and 150 kHz in five ports,'' J. Acoust. Soc. Am. **49**, 928–930 (1971).

[15] F. A. Everest, R. W. Young, and M. W. Johnson, ''Acoustical characteristics of noise produced by snapping shrimp,'' J. Acoust. Soc. Am. **20**, 137–142 (1948).

[16] D. H. Cato and M. J. Bell, ''Ultrasonic ambient noise in Australian shallow waters at frequencies up to 200 kHz,'' Report No. MRL-TR-91-23, Defence Science and Technology Organisation, Materials Research Laboratory, Sydney (1992).

[17] G. C. Jensen, ''Pacific Coast Crabs and Shrimps'' (Sea Challengers, Monterey, 1995).

[18] M. W. Johnson, F. A. Everest, and R. W. Young, ''The role of snapping shrimp (Crangon and Synalpheus) in the production of underwater noise in the sea,'' Biological Bulletin **93**, 122–138 (1947).

[19] D. Ross, *Mechanics of Underwater Noise* (Pergamon, New York, 1976).

[20] D. M. Farmer and S. Vagle, ''Observations of high frequency ambient sound generated by wind,'' in *Sea Surface Sound* (Kluwer, Dordrecht, 1988), pp. 403–416.

[21] Naval Oceanographic Office, ''Shallow water ambient noise levels in the Tongue of the Ocean, Bahamas, Fall of 1965 and Summer of 1966,'' Report No. IR No. 69–57 (1969).

[22] K. S. N. Namboodiripad, ''Acoustical ambient noise of the Cochin Backwaters,'' Indian J. Marine Sci. **7**, 75–78 (1978).

[23] J. Ahn, E. Hamada, and K. Saito, ''Study on the positioning of snapping shrimp and source levels of their sounds,'' Tokyo Univ. Fisheries **80**, 75–81 (1993).

[24] M. Readhead, ''The distribution of snapping shrimp noise near Gladstone, Queensland,'' Report number DSTO-TR-0047, Defence Science and Technology Organisation, Sydney (1994).